

Iris Recognition: An Emerging Biometric Technology

RICHARD P. WILDES, MEMBER, IEEE

This paper examines automated iris recognition as a biometrically based technology for personal identification and verification. The motivation for this endeavor stems from the observation that the human iris provides a particularly interesting structure on which to base a technology for noninvasive biometric assessment. In particular, the biomedical literature suggests that irises are as distinct as fingerprints or patterns of retinal blood vessels. Further, since the iris is an overt body, its appearance is amenable to remote examination with the aid of a machine vision system. The body of this paper details issues in the design and operation of such systems. For the sake of illustration, extant systems are described in some amount of detail.

Keywords—Biometrics, iris recognition, machine vision, object recognition, pattern recognition.

I. INTRODUCTION

A. Motivation

Technologies that exploit biometrics have the potential for application to the identification and verification of individuals for controlling access to secured areas or materials.¹ A wide variety of biometrics have been marshaled in support of this challenge. Resulting systems include those based on automated recognition of retinal vasculature, fingerprints, hand shape, handwritten signature, and voice [24], [40]. Provided a highly cooperative operator, these approaches have the potential to provide acceptable performance. Unfortunately, from the human factors point of view, these methods are highly invasive: Typically, the operator is required to make physical contact with a sensing device or otherwise take some special action (e.g., recite a specific phonemic sequence). Similarly, there is little potential for covert evaluation. One possible alternative to these methods that has the potential to be less invasive is automated face recognition. However, while automated face recognition is a topic of active research, the inherent

difficulty of the problem might prevent widely applicable technologies from appearing in the near term [9], [45]. Automated iris recognition is yet another alternative for noninvasive verification and identification of people. Interestingly, the spatial patterns that are apparent in the human iris are highly distinctive to an individual [1], [34] (see, e.g., Fig. 1). Like the face, the iris is an overt body that is available for remote (i.e., noninvasive) assessment. Unlike the human face, however, the variability in appearance of any one iris might be well enough constrained to make possible an automated recognition system based on currently available machine vision technologies.

B. Background

The word *iris* dates from classical times (*ιρις*, a rainbow). As applied to the colored portion of the exterior eye, iris seems to date to the sixteenth century and was taken to denote this structure's variegated appearance [50]. More technically, the iris is part of the uveal, or middle, coat of the eye. It is a thin diaphragm stretching across the anterior portion of the eye and supported by the lens (see Fig. 2). This support gives it the shape of a truncated cone in three dimensions. At its base, the iris is attached to the eye's ciliary body. At the opposite end, it opens into the pupil, typically slightly to the nasal side and below center. The cornea lies in front of the iris and provides a transparent protective covering.

To appreciate the richness of the iris as a pattern for recognition, it is useful to consider its structure in a bit more detail. The iris is composed of several layers. Its posterior surface consists of heavily pigmented epithelial cells that make it light tight (i.e., impenetrable by light). Anterior to this layer are two cooperative muscles for controlling the pupil. Next is the stromal layer, consisting of collagenous connective tissue in arch-like processes. Coursing through this layer are radially arranged corkscrew-like blood vessels. The most anterior layer is the anterior border layer, differing from the stroma in being more densely packed, especially with individual pigment cells called chromatophores. The visual appearance of the iris is a direct result of its multilayered structure. The anterior surface of the iris is seen to be divided into a

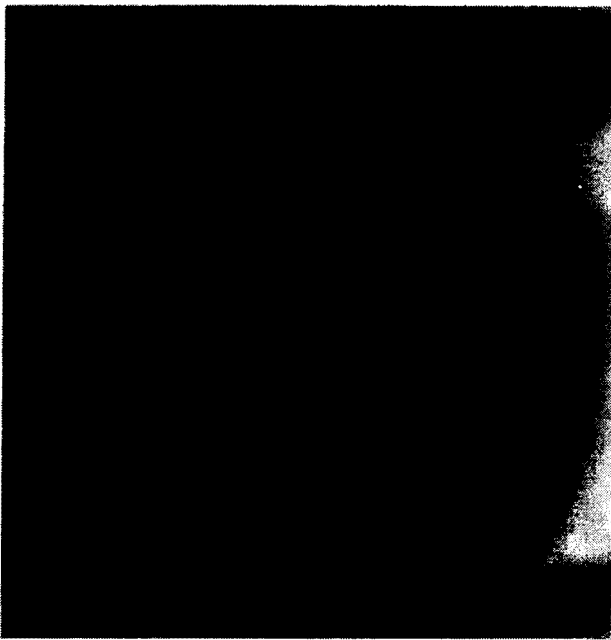
Manuscript received October 31, 1996; revised February 15, 1997. This work was supported in part by The Sarnoff Corporation and in part by The National Information Display Laboratory.

The author is with The Sarnoff Corporation, Princeton, NJ 08543-5300. Publisher Item Identifier S 0018-9219(97)06634-6.

¹ Throughout this discussion, the term "verification" will refer to recognition relative to a specified data base entry. The term "identification" will refer to recognition relative to a larger set of alternative entries.



(a)



(b)

Fig. 1. The distinctiveness of the human iris. The two panels show images of the left iris of two individuals. Even to casual inspection, the imaged patterns in the two irises are markedly different.

central pupillary zone and a surrounding ciliary zone. The border of these two areas is termed the collarette; it appears as a zigzag circumferential ridge resulting as the anterior border layer ends abruptly near the pupil. The ciliary zone contains many interlacing ridges resulting from stromal support. Contractile lines here can vary with the state of the pupil. Additional meridional striations result from the radiating vasculature. Other assorted variations in appearance owe to crypts (irregular atrophy of the border layer), nevi (small elevations of the border layer), and

freckles (local collections of chromatophores). In contrast, the pupillary zone can be relatively flat. However, it often shows radiating spoke-like processes and a pigment frill where the posterior layer's heavily pigmented tissue shows at the pupil boundary. Last, iris color results from the differential absorption of light impinging on the pigmented cells in the anterior border layer. When there is little pigmentation in the anterior border layer, light reflects back from the posterior epithelium and is scattered as it passes through the stroma to yield a blue appearance. Progressive levels of anterior pigmentation lead to darker colored irises. Additional details of iris structure can be found in the biomedical literature (e.g., [1], [16]).

Claims that the structure of the iris is unique to an individual and is stable with age come from two main sources. The first source of evidence is clinical observations. During the course of examining large numbers of eyes, ophthalmologists [20] and anatomists [1] have noted that the detailed pattern of an iris, even the left and right iris of a single person, seems to be highly distinctive. Further, in cases with repeated observations, the patterns seem to vary little, at least past childhood. The second source of evidence is developmental biology [35], [38]. There, one finds that while the general structure of the iris is genetically determined, the particulars of its minutiae are critically dependent on circumstances (e.g., the initial conditions in the embryonic precursor to the iris). Therefore, they are highly unlikely to be replicated via the natural course of events. Rarely, the developmental process goes awry, yielding only a rudimentary iris (aniridia) or a marked displacement (corectopia) or shape distortion (coloboma) of the pupil [35], [42]. Developmental evidence also bears on issues of stability with age. Certain parts of the iris (e.g., the vasculature) are largely in place at birth, whereas others (e.g., the musculature) mature around two years of age [1], [35]. Of particular significance for the purposes of recognition is the fact that pigmentation patterning continues until adolescence [1], [43], [51]. Also, the average pupil size (for an individual) increases slightly until adolescence [1]. Following adolescence, the healthy iris varies little for the rest of a person's life, although slight depigmentation and shrinking of the average pupillary opening are standard with advanced age [1], [42]. Various diseases of the eye can drastically alter the appearance of the iris [41], [42]. It also appears that intensive exposure to certain environmental contaminants (e.g., metals) can alter iris pigmentation [41], [42]. However, these conditions are rare. Claims that the iris changes with more general states of health (iridology) have been discredited [4], [56]. On the whole, these lines of evidence suggest that the iris is highly distinctive and, following childhood, typically stable. Nevertheless, it is important to note that large-scale studies that specifically address the distinctiveness and stability of the iris, especially as a biometric, have yet to be performed.

Another interesting aspect of the iris from a biometric point of view has to do with its moment-to-moment dynamics. Due to the complex interplay of the iris' muscles, the diameter of the pupil is in a constant state of small

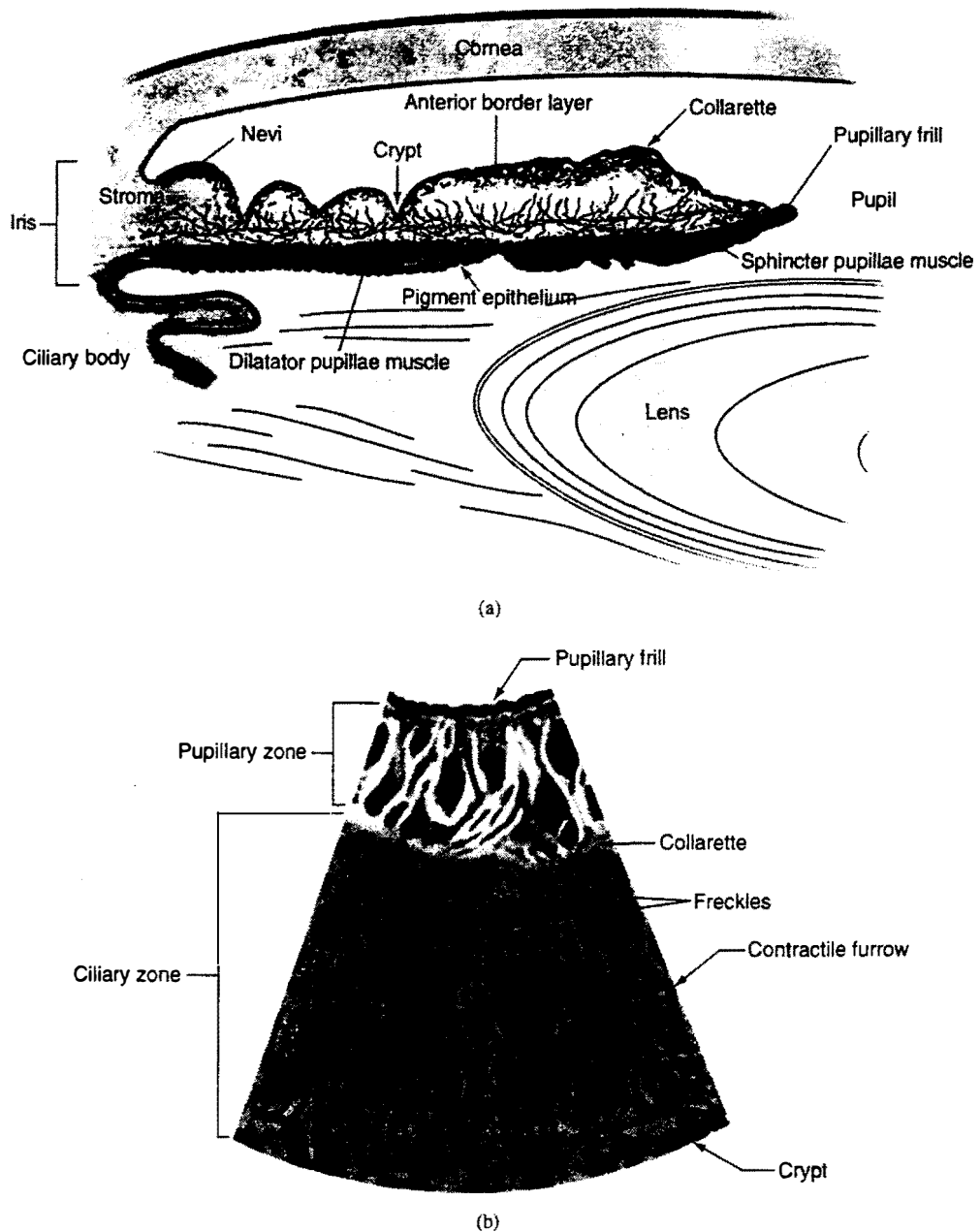


Fig. 2. Anatomy of the human iris. (a) The structure of the iris seen in a transverse section. (b) The structure of the iris seen in a frontal sector. The visual appearance of the human iris derives from its anatomical structure.

oscillation [1], [16]. Potentially, this movement could be monitored to make sure that a live specimen is being evaluated. Further, since the iris reacts very quickly to changes in impinging illumination (e.g., on the order of hundreds of milliseconds for contraction), monitoring the reaction to a controlled illuminant could provide similar evidence. In contrast, upon morbidity, the iris contracts and hardens, facts that may have ramifications for its use in forensics.

Apparently, the first use of iris recognition as a basis for personal identification goes back to efforts to distinguish inmates in the Parisian penal system by visually inspecting their irises, especially the patterning of color [5]. More recently, the concept of automated iris recognition was

proposed by Flom and Safir [20]. It does not appear, however, that this team ever developed and tested a working system. Early work toward actually realizing a system for automated iris recognition was carried out at Los Alamos National Laboratories, CA [32]. Subsequently, two research groups developed and documented prototype iris-recognition systems [14], [52]. These systems have shown promising performance on diverse data bases of hundreds of iris images. Other research into automated iris recognition has been carried out in North America [48] and Europe [37]; however, these efforts have not been well documented to date. More anecdotally, a notion akin to automated iris recognition came to popular attention in the James Bond film *Never Say Never Again*, in which characters are

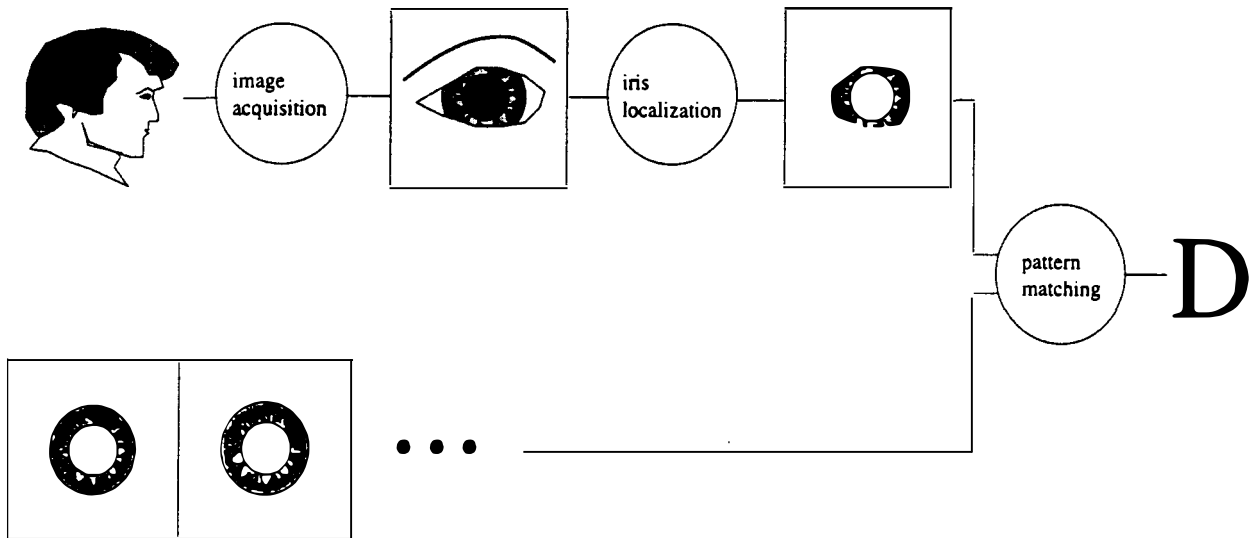


Fig. 3. Schematic diagram of iris recognition. Given a subject to be evaluated (left of upper row) relative to a data base of iris records (left of lower row), recognition proceeds in three steps. The first step is image acquisition, which yields an image of the subject's eye region. The second step is iris localization, which delimits the iris from the rest of the acquired image. The third step is pattern matching, which produces a decision, "D." For verification, the decision is a yes/no response relative to a particular prespecified data base entry; for identification, the decision is a record (possibly null) that has been indexed relative to a larger set of entries.

depicted having images of their eye captured for the purpose of identification [22].

C. Outline

This paper subdivides into four major sections. This first section has served to introduce the notion of automated iris recognition. Section II describes the major technical issues that must be confronted in the design of an iris-recognition system. Illustrative solutions are provided by reference to the two systems that have been well documented in the open literature [14], [52]. Section III overviews the status of these systems, including test results. Last, Section IV provides concluding observations.

II. TECHNICAL ISSUES

Conceptually, issues in the design and implementation of a system for automated iris recognition can be subdivided into three parts (see Fig. 3). The first set of issues surrounds image acquisition. The second set is concerned with localizing the iris per se from a captured image. The third part is concerned with matching an extracted iris pattern with candidate data base entries. This section of the paper discusses these issues in some detail. Throughout the discussion, the iris-recognition systems of Daugman [12]–[14] and Wildes *et al.* [52]–[54] will be used to provide illustrations.

A. Image Acquisition

One of the major challenges of automated iris recognition is to capture a high-quality image of the iris while remaining noninvasive to the human operator. Given that the iris is a relatively small (typically about 1 cm in diameter), dark object and that human operators are very sensitive about

their eyes, this matter requires careful engineering. Several points are of particular concern. First, it is desirable to acquire images of the iris with sufficient resolution and sharpness to support recognition. Second, it is important to have good contrast in the interior iris pattern without resorting to a level of illumination that annoys the operator, i.e., adequate intensity of source (W/cm^2) constrained by operator comfort with brightness ($W/sr\text{-}cm^2$). Third, these images must be well framed (i.e., centered) without unduly constraining the operator (i.e., preferably without requiring the operator to employ an eye piece, chin rest, or other contact positioning that would be invasive). Further, as an integral part of this process, artifacts in the acquired images (e.g., due to specular reflections, optical aberrations, etc.) should be eliminated as much as possible. Schematic diagrams of two image-acquisition rigs that have been developed in response to these challenges are shown in Fig. 4.

Extant iris-recognition systems have been able to answer the challenges of image resolution and focus using standard optics. The Daugman system captures images with the iris diameter typically between 100 and 200 pixels from a distance of 15–46 cm using a 330-mm lens. Similarly, the Wildes *et al.* system images the iris with approximately 256 pixels across the diameter from 20 cm using an 80-mm lens. Due to the need to keep the illumination level relatively low for operator comfort, the optical aperture cannot be too small (e.g., f -stop 11). Therefore, both systems have fairly small depths of field, approximately 1 cm. Video rate capture is exploited by both systems. Typically, this is sufficient to guard against blur due to eye movements provided that the operator is attempting to maintain a steady gaze. Empirically, the overall spatial resolution and focus that results from these designs appear to be sufficient to sup-

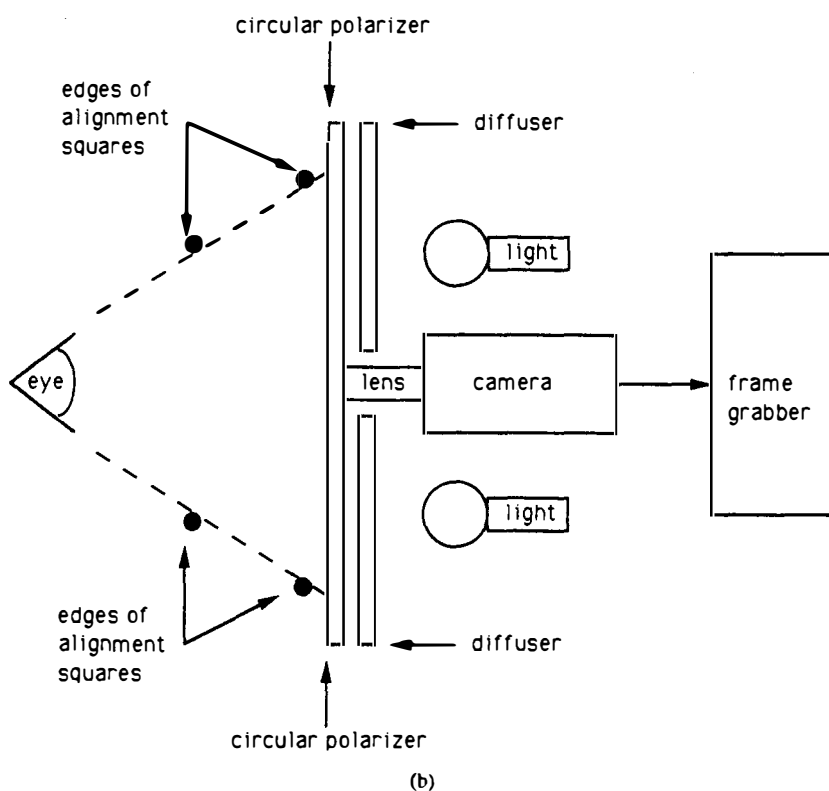
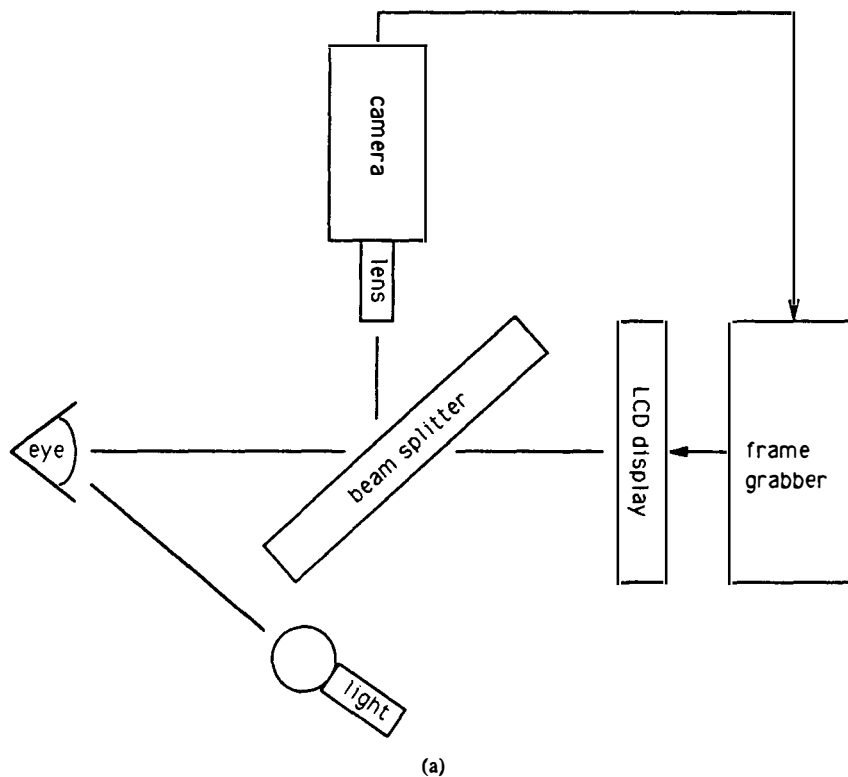


Fig. 4. Image-acquisition rigs for automated iris recognition. (a) A schematic diagram of the Daugman image-acquisition rig. (b) A schematic diagram of the Wildes *et al.* image-acquisition rig.

port iris recognition. Interestingly, additional investigations have shown that images of potential quality to support iris recognition can be acquired in rather different settings. For example, iris images can be acquired at distances up to a meter (using a standard video camera with a telephoto lens) [54]. Further, iris images can be acquired at very close range

while an operator wears a head-mounted display equipped with light emitting diode (LED) illuminants and micro-miniature optics and camera [47]. However, iris images acquired in these latter fashions have received only very preliminary testing with respect to their ability to support recognition.

Illumination of the iris must be concerned with the trade-off between revealing the detail in a potentially low contrast pattern (i.e., due to dense pigmentation of dark irises) and the light sensitivity of human operators. The Daugman and Wildes *et al.* systems illustrate rather different approaches to this challenge. The former makes use of an LED-based point light source in conjunction with a standard video camera. The latter makes use of a diffuse source and polarization in conjunction with a low-light level camera. The former design results in a particularly simple and compact system. Further, by careful positioning of the light source below the operator, reflections of the point source off eyeglasses can be avoided in the imaged iris. Without placing undue restriction on the operator, however, it has not been possible to reliably position the specular reflection at the eye's cornea outside the iris region. Therefore, this design requires that the region of the image where the point source is seen (the lower quadrant of the iris as the system has been instantiated) must be omitted during matching since it is dominated by artifact. The latter design results in an illumination rig that is more complex; however, certain advantages result. First, the use of matched circular polarizers at the light source and the camera essentially eliminates the specular reflection of the light source.² This allows for more of the iris detail to be available for subsequent processing. Second, the coupling of a low light level camera (a silicon intensified camera [26]) with a diffuse illuminant allows for a level of illumination that is entirely unobjectionable to human operators. In terms of spectral distribution, both systems make use of light that is visible to human operators. It has been suggested, however, that infrared illumination would also suffice [14], [47]. Further, both systems essentially eschew color information in their use of monochrome cameras with 8-b gray-level resolution. Presumably, color information could provide additional discriminatory power. Also, color could be of use for initial coarse indexing through large iris data bases. For now, it is interesting to note that empirical studies to date suggest the adequacy of gray-level information alone (see, e.g., Section III).

The positioning of the iris for image capture is concerned with framing all of the iris in the camera's field of view with good focus. Both the Daugman and Wildes *et al.* systems require the operator to self-position his eye region in front of the camera. Daugman's system provides the operator with live video feedback via a miniature liquid-crystal display placed in line with the camera's optics via a beam splitter. This allows the operator to see what the camera is capturing and to adjust his position accordingly.

²Light emerging from the circular polarizer will have a particular sense of rotation. When this light strikes a specularly reflecting surface (e.g., the cornea), the light that is reflected back is still polarized but has reversed sense. This reversed-sense light is not passed through the camera's filter and is thereby blocked from forming an image. In contrast, the diffusely reflecting parts of the eye (e.g., the iris) scatter the impinging light. This light is passed through the camera's filter and is subsequently available for image formation [31]. Interestingly, a similar solution using crossed polarizers (e.g., vertical at the illuminant and horizontal at the camera) is not appropriate for this application: the birefringence of the eye's cornea yields a low-frequency artifact in the acquired images [10].

During this process, the system is continually acquiring images. Once a series of images of sufficient quality is acquired, one is automatically forwarded for subsequent processing. Image quality is assessed by looking for high-contrast edges marking the boundary between the iris and the sclera.

In contrast, the Wildes *et al.* system provides a reticle to aid the operator in positioning. In particular, a square contour is centered around the camera lens so that it is visible to the operator. Suspended in front of this contour is a second, smaller contour of the same shape. The relative sizes and positions of these contours are chosen so that when the eye is in an appropriate position, the squares overlap and appear as one to the operator. As the operator maneuvers, the relative misalignment of the squares provides continuous feedback regarding the accuracy of the current position. Once the operator has completed the alignment, he activates the image capture by pressing a button.

Subjectively, both of the described approaches to positioning are fairly easy for a human operator to master. Since the potential for truly noninvasive assessment is one of the intriguing aspects of iris recognition, however, it is worth underlining the degree of operator participation that is required in these systems. While physical contact is avoided, the level of required cooperativity may still prevent the systems from widespread application. In fact, it appears that all extant approaches to automated iris recognition require operator assistance for this purpose (i.e., as additionally reported in [32], [37], and [48]). Therefore, an interesting direction for future research involves the development of a system that automatically frames an operator's iris over a larger three-dimensional volume with minimal operator participation. For example, the ability to locate a face within a range of about a meter and then to point and zoom a camera to acquire an image of the eye region has been demonstrated using available computer vision technology [23]. While this work is quite preliminary, it suggests the possibility of acquiring iris images in scenarios that are more relaxed than those required by current iris-recognition systems. The ability to perform this task in an effective and efficient manner is likely to have great implications for the widespread deployment of iris recognition.

For graphical illustration, an image of an iris, including the surrounding eye region, is shown in Fig. 5. The quality of this image, acquired from the Wildes *et al.* system, could be expected from either of the systems under discussion.

B. Iris Localization

Without placing undue constraints on the human operator, image acquisition of the iris cannot be expected to yield an image containing only the iris. Rather, image acquisition will capture the iris as part of a larger image that also contains data derived from the immediately surrounding eye region. Therefore, prior to performing iris pattern matching, it is important to localize that portion of the acquired image that corresponds to an iris. In particular, it is necessary to localize that portion of the image derived from inside the limbus (the border between the sclera and the iris) and



Fig. 5. Example of captured iris image. Imaging of the iris must acquire sufficient detail for recognition while being minimally invasive to the operator. Image acquisition yields an image of the iris as well as the surrounding eye region.

outside the pupil. Further, if the eyelids are occluding part of the iris, then only that portion of the image below the upper eyelid and above the lower eyelid should be included. Typically, the limbic boundary is imaged with high contrast, owing to the sharp change in eye pigmentation that it marks. The upper and lower portions of this boundary, however, can be occluded by the eyelids. The pupillary boundary can be far less well defined. The image contrast between a heavily pigmented iris and its pupil can be quite small. Further, while the pupil typically is darker than the iris, the reverse relationship can hold in cases of cataract: the clouded lens leads to a significant amount of backscattered light. Like the pupillary boundary, eyelid contrast can be quite variable depending on the relative pigmentation in the skin and the iris. The eyelid boundary also can be irregular due to the presence of eyelashes. Taken in tandem, these observations suggest that iris localization must be sensitive to a wide range of edge contrasts, robust to irregular borders, and capable of dealing with variable occlusion.

Reference to how the Daugman and Wildes *et al.* iris-recognition systems perform iris localization further illustrates the issues. Both of these systems make use of first derivatives of image intensity to signal the location of edges that correspond to the borders of the iris. Here, the notion is that the magnitude of the derivative across an imaged border will show a local maximum due to the local change of image intensity. Also, both systems model the various boundaries that delimit the iris with simple geometric models. For example, they both model the limbus and pupil with circular contours. The Wildes *et al.* system also explicitly models the upper and lower eyelids with parabolic arcs, whereas the Daugman system simply excludes the upper- and lower-most portions of the image, where eyelid occlusion is expected to occur. In both systems, the expected configuration of model components is used to fine tune the image intensity derivative information. In particular, for the limbic boundary, the derivatives are filtered to be selective for vertical edges. This directional selectivity is motivated by the fact that even in the face of

occluding eyelids, the left and right portions of the limbus should be visible and oriented near the vertical (assuming that the head is in an upright position). Similarly, the derivatives are filtered to be selective for horizontal information when locating the eyelid borders. In contrast, since the entire (roughly circular) pupillary boundary is expected to be present in the image, the derivative information is used in a more isotropic fashion for localization of this structure. In practice, this fine tuning of the image information has proven to be critical for accurate localization. For example, without such tuning, the fits can be driven astray by competing image structures (e.g., eyelids interfering with limbic localization, etc.).

The two systems differ mostly in the way that they search their parameter spaces to fit the contour models to the image information. To understand how these searches proceed, let $I(x, y)$ represent the image intensity value at location (x, y) and let circular contours (for the limbic and pupillary boundaries) be parameterized by center location (x_c, y_c) and radius r . The Daugman system fits the circular contours via gradient ascent on the parameters (x_c, y_c, r) so as to maximize

$$\left| \frac{\partial}{\partial r} G(r) * \oint_{r, x_c, y_c} \frac{I(x, y)}{2\pi r} ds \right|$$

where $G(r) = (1/\sqrt{2\pi}\sigma)e^{-((r-r_0)^2/2\sigma^2)}$ is a radial Gaussian with center r_0 and standard deviation σ that smooths the image to select the spatial scale of edges under consideration, $*$ symbolizes convolution, ds is an element of circular arc, and division by $2\pi r$ serves to normalize the integral. In order to incorporate directional tuning of the image derivative, the arc of integration ds is restricted to the left and right quadrants (i.e., near vertical edges) when fitting the limbic boundary. This arc is considered over a fuller range when fitting the pupillary boundary; however, the lower quadrant of the image is still omitted due to the artifact of the specular reflection of the illuminant in that region (see Section II-A). In implementation, the contour fitting procedure is discretized, with finite differences serving for derivatives and summation used to instantiate integrals and convolutions. More generally, fitting contours to images via this type of optimization formulation is a standard machine vision technique, often referred to as active contour modeling (see, e.g., [33] and [57]).

The Wildes *et al.* system performs its contour fitting in two steps. First, the image intensity information is converted into a binary edge-map. Second, the edge points vote to instantiate particular contour parameter values. The edge-map is recovered via gradient-based edge detection [2], [44]. This operation consists of thresholding the magnitude of the image intensity gradient, i.e., $|\nabla G(x, y) * I(x, y)|$, where $\nabla \equiv (\partial/\partial x, \partial/\partial y)$ while

$$G(x, y) = \frac{1}{2\pi\sigma^2} e^{-\frac{(x-x_0)^2 + (y-y_0)^2}{2\sigma^2}}$$

is a two-dimensional Gaussian with center (x_0, y_0) and standard deviation σ that smooths the image to select the

spatial scale of edges under consideration. In order to incorporate directional tuning, the image intensity derivatives are weighted to favor certain ranges of orientation prior to taking the magnitude. For example, prior to contributing to the fit of the limbic boundary contour, the derivatives are weighted to be selective for vertical edges. The voting procedure is realized via Hough transforms [27], [28] on parametric definitions of the iris boundary contours. In particular, for the circular limbic or pupillary boundaries and a set of recovered edge points (x_j, y_j) , $j = 1, \dots, n$, a Hough transform is defined as

$$H(x_c, y_c, r) = \sum_{j=1}^n h(x_j, y_j, x_c, y_c, r)$$

where

$$h(x_j, y_j, x_c, y_c, r) = \begin{cases} 1, & \text{if } g(x_j, y_j, x_c, y_c, r) = 0 \\ 0, & \text{otherwise} \end{cases}$$

with

$$g(x_j, y_j, x_c, y_c, r) = (x_j - x_c)^2 + (y_j - y_c)^2 - r^2.$$

For each edge point (x_j, y_j) , $g(x_j, y_j, x_c, y_c, r) = 0$ for every parameter triple (x_c, y_c, r) that represents a circle through that point. Correspondingly, the parameter triple that maximizes H is common to the largest number of edge points and is a reasonable choice to represent the contour of interest. In implementation, the maximizing parameter set is computed by building $H(x_c, y_c, r)$ as an array that is indexed by discretized values for x_c , y_c , and r . Once populated, the array is scanned for the triple that defines its largest value. Contours for the upper and lower eyelids are fit in a similar fashion using parameterized parabolic arcs in place of the circle parameterization $g(x_j, y_j, x_c, y_c, r)$. Just as the Daugman system relies on standard techniques for iris localization, edge detection followed by a Hough transform is a standard machine vision technique for fitting simple contour models to images [2], [44].

Both approaches to localizing the iris have proven to be successful in the targeted application. The histogram-based approach to model fitting should avoid problems with local minima that the active contour model's gradient descent procedure might experience. By operating more directly with the image derivatives, however, the active contour approach avoids the inevitable thresholding involved in generating a binary edge-map. Further, explicit modeling of the eyelids (as done in the Wildes *et al.* system) should allow for better use of available information than simply omitting the top and bottom of the image. However, this added precision comes with additional computational expense. More generally, both approaches are likely to encounter difficulties if required to deal with images that contain broader regions of the surrounding face than the immediate eye region. For example, such images are likely to result from image-acquisition rigs that require less operator participation than those currently in place. Here, the additional image "clutter" is likely to drive the current, relatively simple model fitters to poor results. Solutions to

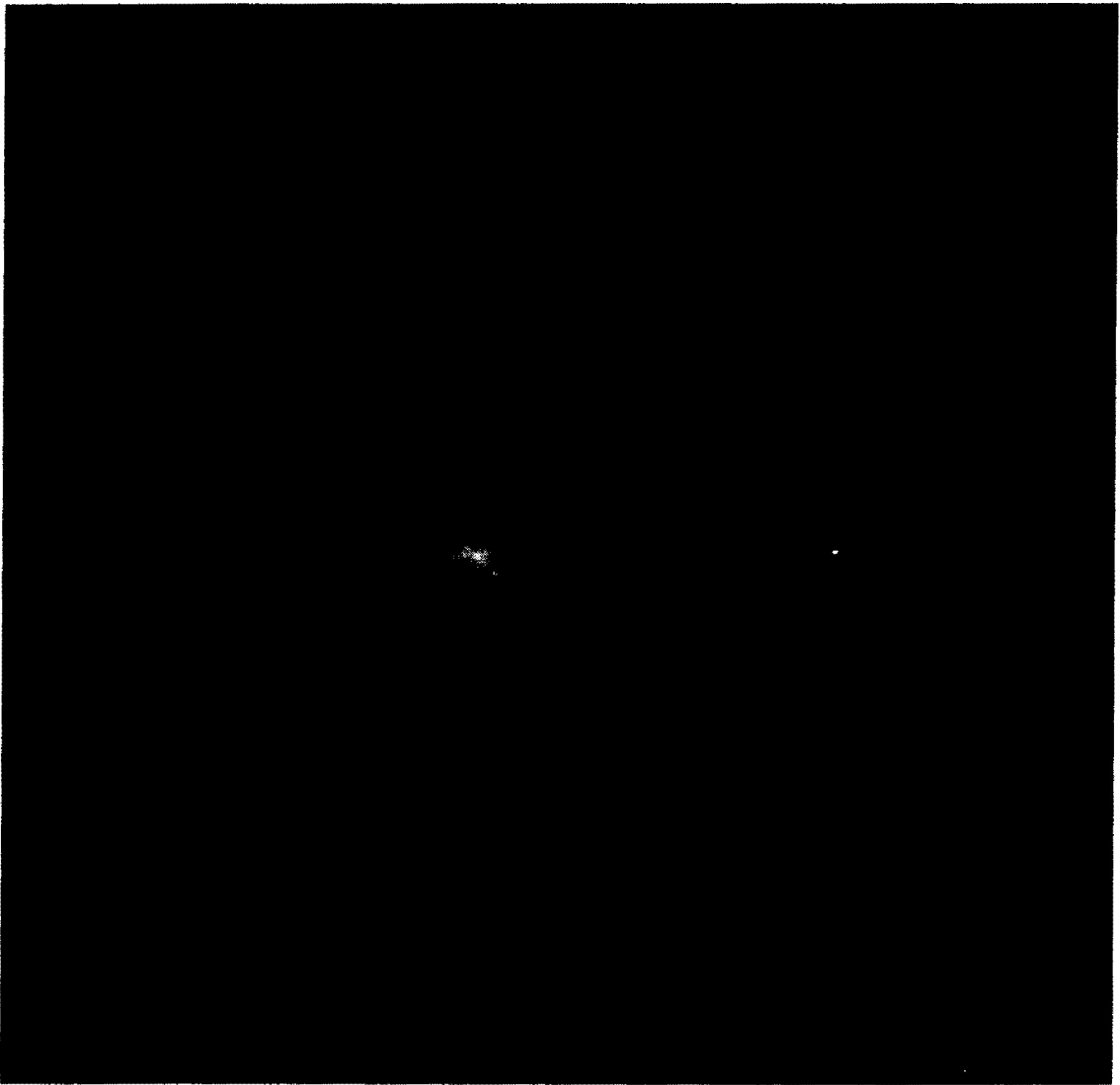


Fig. 6. Illustrative results of iris localization. Given an acquired image, it is necessary to separate the iris from the surround. The input to the localization process was the captured iris image of Fig. 5. Following iris localization, all but the iris per se is masked out.

this type of situation most likely will entail a preliminary coarse eye localization procedure to seed iris localization proper. In any case, following successful iris localization, the portion of the captured image that corresponds to the iris can be delimited. Fig. 6 provides an example result of iris localization as performed by the Wildes *et al.* system.

C. Pattern Matching

Having localized the region of an acquired image that corresponds to the iris, the final task is to decide if this pattern matches a previously stored iris pattern. This matter of pattern matching can be decomposed into four parts:

- 1) bringing the newly acquired iris pattern into spatial alignment with a candidate data base entry;
- 2) choosing a representation of the aligned iris patterns that makes their distinctive patterns apparent;
- 3) evaluating the goodness of match between the newly acquired and data base representations;

- 4) deciding if the newly acquired data and the data base entry were derived from the same iris based on the goodness of match.

1) Alignment: To make a detailed comparison between two images, it is advantageous to establish a precise correspondence between characteristic structures across the pair. Both of the systems under discussion compensate for image shift, scaling, and rotation. Given the systems' ability to aid operators in accurate self-positioning, these have proven to be the key degrees of freedom that required compensation. Shift accounts for offsets of the eye in the plane parallel to the camera's sensor array. Scale accounts for offsets along the camera's optical axis. Rotation accounts for deviation in angular position about the optical axis. Nominally, pupil dilation is not a critical issue for the current systems since their constant controlled illumination should bring the pupil of an individual to the same size across trials (barring illness, etc.). For both systems, iris localization is charged with isolating an iris in a larger acquired image and

thereby essentially accomplishes alignment for image shift. Daugman's system uses radial scaling to compensate for overall size as well as a simple model of pupil variation based on linear stretching. This scaling serves to map Cartesian image coordinates (x, y) to dimensionless polar image coordinates (r, θ) according to

$$\begin{aligned} x(r, \theta) &= (1 - r)x_p(\theta) + rx_l(\theta) \\ y(r, \theta) &= (1 - r)y_p(\theta) + ry_l(\theta) \end{aligned}$$

where r lies on $[0, 1]$ and θ is cyclic over $[0, 2\pi]$, while $(x_p(\theta), y_p(\theta))$ and $(x_l(\theta), y_l(\theta))$ are the coordinates of the pupillary and limbic boundaries in the direction θ . Rotation is compensated for by explicitly shifting an iris representation in θ by various amounts during matching.

The Wildes *et al.* system uses an image-registration technique to compensate for both scaling and rotation. This approach geometrically warps a newly acquired image $I_a(x, y)$ into alignment with a selected data base image $I_d(x, y)$ according to a mapping function $(u(x, y), v(x, y))$ such that for all (x, y) , the image intensity value at $(x, y) - (u(x, y), v(x, y))$ in I_a is close to that at (x, y) in I_d . More precisely, the mapping function (u, v) is taken to minimize

$$\int_x \int_y (I_d(x, y) - I_a(x - u, y - v))^2 dx dy$$

while being constrained to capture a similarity transformation of image coordinates (x, y) to (x', y') , i.e.,

$$\begin{pmatrix} x' \\ y' \end{pmatrix} = \begin{pmatrix} x \\ y \end{pmatrix} - sR(\phi) \begin{pmatrix} x \\ y \end{pmatrix}$$

with s a scaling factor and $R(\phi)$ a matrix representing rotation by ϕ . In implementation, given a pair of iris images I_a and I_d , the warping parameters s and ϕ , are recovered via an iterative minimization procedure [3].

As with much of the processing that the two iris-recognition systems perform, the methods for establishing correspondences between acquired and data base iris images seem to be adequate for controlled assessment scenarios. Once again, however, more sophisticated methods may prove to be necessary in more relaxed scenarios. For example, a simple linear stretching model of pupil dilation does not capture the complex physical nature of this process, e.g., the coiling of blood vessels and the arching of stromal fibers. Similarly, more complicated global geometric compensations will be necessary if full perspective distortions (e.g., foreshortening) become significant.

2) Representation: The distinctive spatial characteristics of the human iris are manifest at a variety of scales. For example, distinguishing structures range from the overall shape of the iris to the distribution of tiny crypts and detailed texture. To capture this range of spatial detail, it is advantageous to make use of a multiscale representation. Both of the iris-recognition systems under discussion make use of bandpass image decompositions to avail themselves of multiscale information. The Daugman system makes use of a decomposition derived from application of a two-dimensional version of Gabor filters [21] to the image data.

Since the Daugman system converts to polar coordinates (r, θ) during alignment, it is convenient to give the filters in a corresponding form as

$$H(r, \theta) = e^{-i\omega(\theta - \theta_0)} e^{-(r - r_0)^2 / \alpha^2} e^{-i(\theta - \theta_0)^2 / \beta^2}$$

where α and β covary in inverse proportion to ω to generate a set of quadrature pair frequency-selective filters with center locations specified by (r_0, θ_0) . These filters are particularly notable for their ability to achieve good joint localization in the spatial and frequency domains. Further, owing to their quadrature nature, these filters can capture information about local phase. Following the Gabor decomposition, Daugman's system compresses its representation by quantizing the local phase angle according to whether the real, $\Re(\cdot)$, and imaginary, $\Im(\cdot)$, filter outputs are positive or negative. For a filter given with bandpass parameters α, β , and ω and location (r_0, θ_0) , a pair of bits (h_{\Re}, h_{\Im}) is generated according to

$$\begin{aligned} h_{\Re} &= 1 \text{ if } \Re \left(\int_{\rho} \int_{\psi} e^{-i\omega(\theta_0 - \psi)} e^{-(r_0 - \rho)^2 / \alpha^2} \right. \\ &\quad \left. \times e^{-i(\theta_0 - \psi)^2 / \beta^2} I(\rho, \psi) \rho d\rho d\psi \right) \geq 0 \\ h_{\Re} &= 0 \text{ if } \Re \left(\int_{\rho} \int_{\psi} e^{-i\omega(\theta_0 - \psi)} e^{-(r_0 - \rho)^2 / \alpha^2} \right. \\ &\quad \left. \times e^{-i(\theta_0 - \psi)^2 / \beta^2} I(\rho, \psi) \rho d\rho d\psi \right) < 0 \\ h_{\Im} &= 1 \text{ if } \Im \left(\int_{\rho} \int_{\psi} e^{-i\omega(\theta_0 - \psi)} e^{-(r_0 - \rho)^2 / \alpha^2} \right. \\ &\quad \left. \times e^{-i(\theta_0 - \psi)^2 / \beta^2} I(\rho, \psi) \rho d\rho d\psi \right) \geq 0 \\ h_{\Im} &= 0 \text{ if } \Im \left(\int_{\rho} \int_{\psi} e^{-i\omega(\theta_0 - \psi)} e^{-(r_0 - \rho)^2 / \alpha^2} \right. \\ &\quad \left. \times e^{-i(\theta_0 - \psi)^2 / \beta^2} I(\rho, \psi) \rho d\rho d\psi \right) < 0. \end{aligned}$$

The parameters $r_0, \theta_0, \alpha, \beta$, and ω are sampled so as to yield a 256-byte representation that serves as the basis for subsequent processing. In implementation, the Gabor filtering is performed via a relaxation algorithm [11], with quantization of the recovered phase information yielding the final representation.

The Wildes *et al.* system makes use of an isotropic bandpass decomposition derived from application of Laplacian of Gaussian filters [25], [29] to the image data. These filters can be specified as

$$-\frac{1}{\pi\sigma^4} \left(1 - \frac{\rho^2}{2\sigma^2} \right) e^{-\rho^2 / 2\sigma^2}$$

with σ the standard deviation of the Gaussian and ρ the radial distance of a point from the filter's center. In practice, the filtered image is realized as a Laplacian pyramid [8], [29]. This representation is defined procedurally in terms of a cascade of small Gaussian-like filters. In particular, let $\mathbf{w} = [1 \ 4 \ 6 \ 4 \ 1]/16$ be a one-dimensional mask and $\mathbf{W} = \mathbf{w}^T \mathbf{w}$ be the two-dimensional mask that results from



Fig. 7. Multiscale representation for iris pattern matching. Distinctive features of the iris are manifest across a range of spatial scales. Pattern matching is well served by a bandpass decomposition spanning high to low spatial frequency. A compact representation results from successive subsampling of lower frequency bands. The localized iris of Fig. 6 is shown under such a multiscale representation.

taking the outer product of w with itself. Given an image of interest I , construction of a Laplacian pyramid begins with convolution of I with W so as to yield a set of low-pass filtered images g_k according to

$$g_k = (W * g_{k-1})_{\downarrow 2}$$

with $g_0 = I$ and $(\cdot)_{\downarrow 2}$ symbolizing down sampling by a factor of two in each image dimension. The k th level of the Laplacian pyramid l_k is formed as the difference between g_k and g_{k+1} , with g_{k+1} expanded before subtraction so that it matches the sampling rate of g_k . The expansion is accomplished by upsampling and interpolation

$$l_k = g_k - 4W^* * (g_{k+1})_{\uparrow 2}$$

where $(\cdot)_{\uparrow 2}$ indicates upsampling by a factor of two via insertion of a row and column of zeros between each row and column of the original image. The generating kernel W is used as the interpolation filter, and the factor of four is necessary because $3/4$ of the samples in the image are newly inserted zeros. The resulting Laplacian pyramid, constructed with four levels, serves as the basis for subsequent processing. The difference of Gaussians that the construction of this representation entails yields a good approximation to Laplacian of Gaussian filtering [39]. Additionally, it is of note for efficient storage and processing as lower frequency bands are subsampled successively without loss of information beyond that introduced by the filtering. In implementation, Laplacian pyramid construction follows in a straightforward fashion from its procedural definition.

By quantizing its filter outputs, the representational approach that is used in the Daugman system yields a remarkably parsimonious representation of an iris. Indeed,

a representation with a size of 256 bytes can be accommodated on the magnetic stripe affixed to the back of standard credit/debit cards [7]. In contrast, the Wildes *et al.* representation is derived directly from the filtered image for size on the order of the number of bytes in the iris region of the originally captured image. By retaining more of the available iris information, however, the Wildes *et al.* system might be capable of making finer grained distinctions between different irises. Since large-scale studies of iris recognition are currently lacking, it is too early to tell exactly how much information is necessary for adequate discrimination in the face of sizable samples from the human population. In any case, in deriving their representations from bandpass filtering operations, both approaches capitalize on the multiscale structure of the iris. For the sake of illustration, an example multiscale representation of an iris as recovered by the Wildes *et al.* system, is shown in Fig. 7.

3) *Goodness of Match*: Given the systems' controlled image acquisitions and abilities to bring data base entry and newly acquired data into precise alignment, an appropriate match metric can be based on direct point-wise comparisons between primitives in the corresponding representations. The Daugman system quantifies this matter by computing the percentage of mismatched bits between a pair of iris representations, i.e., the normalized Hamming distance [30]. Letting A and B be two iris representations to be compared, this quantity can be calculated as

$$\frac{1}{2048} \sum_{j=1}^{j=2048} A_j \oplus B_j$$

with subscript j indexing bit position and \oplus denoting the exclusive-OR operator. (The exclusive-OR is a Boolean operator that equals one if and only if the two bits A_j and B_j are different.) The result of this computation is then used as the goodness of match, with smaller values indicating better matches. The exclusive-OR of corresponding bits in the acquired and data base iris representations can be calculated with negligible computational expense. This allows the system to compare an acquired representation with interesting numbers of data base entries (e.g., on the order of 10^3) in under a second. The system exploits this comparison rate as a brute force solution to identification, not just verification of an operator, i.e., sequential examination of each record in moderate-size data bases. While this search ability is impressive, identification in the face of significantly larger data bases might require a cleverer indexing strategy.

The Wildes *et al.* system employs a somewhat more elaborate procedure to quantify the goodness of match. The approach is based on normalized correlation between the acquired and data base representations. In discrete form, normalized correlation can be defined in the following fashion. Let $p_1[i, j]$ and $p_2[i, j]$ be two image arrays of size $n \times m$. Further, let $\mu_1 = (1/nm) \sum_{i=1}^n \sum_{j=1}^m p_1[i, j]$ and

$$\sigma_1 = \sqrt{(1/nm) \sum_{i=1}^n \sum_{j=1}^m (p_1[i, j] - \mu_1)^2}$$

be the mean and standard deviation for the intensities of p_1 , respectively. Also, let μ_2 and σ_2 be similarly defined with reference to p_2 . Then, the normalized correlation between p_1 and p_2 can be defined as

$$\frac{\sum_{i=1}^n \sum_{j=1}^m (p_1[i, j] - \mu_1)(p_2[i, j] - \mu_2)}{nm\sigma_1\sigma_2}$$

Normalized correlation captures the same type of information as standard correlation (i.e., integrated similarity of corresponding points in the regions); however, it also accounts for local variations in image intensity that corrupt standard correlation [2]. This robustness comes about as the mean intensities are subtracted in the numerator of the correlation ratio, while the standard deviations appear in the denominator. In implementation, the correlations are performed discretely over small blocks of pixels (8×8) in each of the four spatial frequency bands that are instantiated in the Laplacian pyramid representations. These operations result in multiple correlation values for each band. Subsequent processing combines the block correlations within a band into a single value via the median statistic. In sum, this yields a set of four goodness-of-match values, one for each frequency band. Blocking combined with the median operation allows for local adjustments of matching and a degree of outlier rejection, and thereby provides robustness against mismatches due to noise, misalignment, and occlusion (e.g., a stray eyelash). This method has been applied to the verification task only.

4) *Decision:* The final task that must be performed for current purposes is to evaluate the goodness-of-match values into a final judgment as to whether the acquired data does (authentic) or does not (imposter) come from the same iris as does the data base entry. For the Daugman system, this amounts to choosing a separation point in the space of (normalized) Hamming distances between iris representations. Distances smaller than the separation point will be taken as indicative of authentic; those larger will be taken as indicative of imposters.³ An appeal to statistical decision theory [36], [49] is made to provide a principled approach to selecting the separation point. There, given distributions for the two events to be distinguished (i.e., authentic versus imposter), the optimal decision strategy is defined by taking the separation as the point at which the two distributions cross over. This decision strategy is optimal in the sense that it leads to equal probability of false accept and false reject errors. (Of course, even with a theoretically "optimal" decision point in hand, one is free to choose either a more conservative or more liberal criterion according to the needs of a given installation.) In order to calculate the cross-over point, sample populations of imposters and authentic were each fit with parametrically defined distributions. This was necessary since no data, i.e., Hamming distances, were observed in the cross-over region. Binomial distributions [17] were used for the empirical fits. A binomial distribution is given as

$$p(k) = \binom{n}{k} P^k (1-P)^{n-k}$$

where

$$\binom{n}{k} = \frac{n!}{(n-k)!k!}$$

is the number of k combinations of n distinguishable items. This formula gives the probability of k successes in n independent Bernoulli trials. A Bernoulli trial, in turn, is defined to generate an experimental value of a discrete random variable v according to the distribution

$$p_v(v_0) = \begin{cases} 1-P, & v_0 = 0 \\ P, & v_0 = 1 \\ 0, & \text{otherwise} \end{cases}$$

with an outcome of $v = 1$ taken as a success and an outcome of $v = 0$ taken as a failure. The use of a binomial distribution was justified for the case of imposter matches based on the distinctiveness of different irises. That is, the matching of bits between a pair of representations from different irises was taken to be a series of Bernoulli trials. Not all of the bit matches were taken as independent, however, due to the presence of inherent correlations in iris structure as well as correlations introduced during processing. Significantly, no such justification was given for the modeling of the authentic.

³ As documented, both the Daugman and Wildes *et al.* systems remain agnostic about how to deal with cases that lie at their separation points, where the goodness of match is supposed to be equally supportive of deciding "authentic" or "imposter." In empirical evaluations, it appears that neither system has been confronted with this situation (see Section III).

For the Wildes *et al.* system, the decision-making process must combine the four goodness-of-match measurements that are calculated by the previous stage of processing (i.e., one for each pass band in the Laplacian pyramid representation) into a single accept/reject judgement. Recourse is had in standard techniques from pattern classification. In particular, the notion that is appealed to is to combine the values in a fashion so that the variance within a class of iris data is minimized while the variance between different classes of iris data is maximized. The linear function that provides such a solution is well known and is given by Fisher's linear discriminant [18], [19]. This function can be defined in the following fashion. Let there be n d -dimensional samples q , n_a of which are from a set \mathcal{A} and n_i of which are from a set \mathcal{I} . For example, in the current application, each sample corresponds to a set of multiscale goodness-of-match measurements, while the classes to be distinguished are the authentic and imposters. Fisher's linear discriminant defines a weight vector ω such that the ratio of between class variance to within class variance is maximized for the transformed samples $\omega^T q$. To formalize this notion, let $\mu_a = (\sum_{q \in \mathcal{A}} q)/n_a$ be the d -dimensional mean for $q \in \mathcal{A}$ and similarly for μ_i . A measure of variance within a class of data can be given in terms of a scatter matrix with the form

$$S_a = \sum_{q \in \mathcal{A}} (q - \mu_a)(q - \mu_a)^T$$

for \mathcal{A} and with S_i similarly defined for \mathcal{I} . The total within class scatter is given as $S_w = S_a + S_i$. A corresponding measure of variance between classes can be defined in terms of the scatter matrix

$$S_b = (\mu_a - \mu_i)(\mu_a - \mu_i)^T.$$

With the preceding definitions in hand, the expression

$$\frac{\omega^T S_b \omega}{\omega^T S_w \omega}$$

describes the ratio of between to within class variance of the transformed samples ωq . Last, the use of a bit of calculus and linear algebra leads to the conclusion that the ω that maximizes this ratio is given as

$$\omega = S_w^{-1}(\mu_a - \mu_i).$$

Interestingly, S_b does not appear in this formula for ω since it simply scales the overall result without otherwise changing the separation. To apply this discriminant function to classification, a separation point must be defined in its range. Values above this point will be taken as derived from class \mathcal{A} ; values below this point will be taken as derived from class \mathcal{I} . In the current application, the separation point is taken as the midpoint between the transformed means of the samples from \mathcal{A} and \mathcal{I} , i.e., $(1/2)\omega^T(\mu_a + \mu_i)$. If the probabilities of the measurements given either class are normally distributed and have equal variance, (i.e., $p(q|\mathcal{A}) = 1/\sqrt{2\pi}\sigma e^{-|q-\mu_a|^2/2\sigma^2}$ with σ^2 the variance [17], and similarly for \mathcal{I}), then this choice of separation

point can be shown to be optimal (i.e., equal probability of false accept and false reject errors). It is heuristic for the case of iris match measurements, however, where these assumptions are not known to hold. In implementation, the discriminant was defined empirically based on a set of iris training data.

While both of the decision methods have performed well to date, the underlying data-modeling assumptions need to be rigorously evaluated against a larger corpus of data. Both of the methods rely on the assumptions that the imposter and authentic populations can each be modeled with single distributions. A basic tenet of iris recognition is that different irises are highly distinct. Therefore, it is reasonable to view the distribution of imposters as varying about a central tendency dictated by some notion of independence, e.g., a 50% chance of individual bits' matching in the Daugman representation or poor correlation for the multiscale matches in the Wildes *et al.* system. Indeed, empirically, this seems to be the case for both systems. However, there is no such theoretical underpinning for modeling the authentic with a single distribution. In fact, one might argue that authentic would be best modeled by a mixture of distributions, perhaps even one distribution for repeat occurrences of each iris. From an empirical point of view, it is of concern that the current decision strategies are derived from rather small samples of the population (i.e., on the order of 10^2). This matter is exacerbated by the fact that little data has been reported in the cross-over regions for the decisions, exactly the points of most concern. To resolve these issues properly, it will be necessary to consider a larger sample of iris data than the current systems have employed.

5) *A Caveat:* Both of the reviewed approaches to pattern matching are based on methods that are closely tied to the recorded image intensities. More abstract representations may be necessary to deal with greater variation in the appearance of any one iris, e.g., as might result from more relaxed image acquisition. One way to deal with greater variation would be to extract and match sets of features that are expected to be more robust to photometric and geometric distortions in the acquired images. In particular, features that bear a closer and more explicit relationship to physical structures of the iris might exhibit the desired behavior. For example, preliminary results indicate that multiscale blob matching could be valuable in this regard [54]. This approach relies on the correspondence between the dark and light blob structures that typically are apparent in iris images and iris structures such as crypts, freckles, nevi, and striations. If current methods in iris pattern matching begin to break down in future applications, then such symbolic approaches will deserve consideration. It is worth noting, however, that the added robustness that these approaches might yield will most likely come with increased computational expense.

D. Recapitulation

The main functional components of extant iris-recognition systems consist of image acquisition, iris

localization, and pattern matching. In evaluating designs for these components, one must consider a wide range of technical issues. Chief among these are the physical nature of the iris, optics, image processing/analysis, and human factors. All these considerations must be combined to yield robust solutions even while incurring modest computational expense and compact design. Example solutions to these issues are in place. These solutions have proven to be reliable in preliminary evaluations. More challenging operational scenarios (e.g., acquisition of images with less operator participation) might require somewhat different or at least more elaborate approaches.

III. SYSTEMS AND PERFORMANCE

The image-acquisition, iris-localization, and pattern-matching components developed by Daugman [12]–[14] and Wildes *et al.* [52]–[54] have been assembled into prototype iris-recognition systems. Both of these systems have been awarded U.S. patents [15], [55]. Further, both systems have been the subject of preliminary empirical evaluation. In this section, the system and performance aspects of the two approaches are described.

The Daugman iris-recognition system consists of an image-acquisition rig (standard video camera, lens, framegrabber, LED illuminator and miniature video display for operator positioning) interfaced to a standard computer workstation (a Sun 4). The image-analysis software for the system has been implemented in optimized integer code. The system is capable of three functional modes of operation: enrollment, verification, and identification. In enrollment mode, an image of an operator is captured and a corresponding data base entry is created and stored. In verification mode, an image of an operator is acquired and is evaluated relative to a specified data base entry. In identification mode, an image is acquired and evaluated relative to the entire data base via sequential comparisons. Both the enrollment and verification modes take under 1 s to complete. The identification mode can evaluate against a data base of up to 4000 entries in the same amount of time. A commercial version of this system also is available through IriScan [46]. This version embodies largely the same approach, albeit with further optimization and special-purpose hardware for a more compact instantiation.

The Daugman system has been subjected to two sets of empirical tests. In the first study, 592 irises were represented as derived from 323 persons [14]. An average of approximately three images were taken of each iris. (The time lag involved in repeat captures of a single iris has not been reported.) The irises involved spanned the range of common iris colors: blue, hazel, green, and brown. This preparation allows for evaluation of authentic and imposters across a representative range of iris pigmentations and with some passage of time. In the face of this data set, the system exhibited no false accepts and no false rejects. In an attempt to analyze the data from this experiment, binomial distributions were fit to both the observed authentic and imposter scores, i.e., as previously

described during the discussion of pattern matching. The fits were used to calculate several statistics. The cross-over error rate for false accepts and false rejects was found to be 1 in 131 000. Further, based on the means of the fits, typical matching statistics were calculated. For the “typical” imposter comparison, the confidence with which the operator was rejected corresponded to a conditional false reject probability of 1 in $10^{9.6}$. For the “typical” authentic comparison, the confidence with which the operator was accepted corresponded to a conditional false accept probability of 1 in 10^{31} . Interpretation of these inferences requires caution. As noted during the discussion of pattern matching, justification for fitting the observed data with binomial distributions is problematic. From a theoretical point of view, it is not clear why such a distribution is appropriate for the case of authentic. From an empirical point of view, the fits are based on small samples of the populations, and data is lacking in the critical cross-over region. Nevertheless, it is worth noting that qualitatively, the data for authentic and imposters were well separated in this study.

In a second study, a preproduction version of the commercial IriScan system was evaluated [6]. In this study, the system was installed in a public space at Sandia National Laboratories, NM. Operators consisted of volunteers from the Sandia community. The study was conducted in two phases. In the first phase, 199 irises were represented as derived from 122 people. Following enrollment, the operators made a total of 878 attempts to use the system in identification mode over a period of eight days. Of these attempts, 89 false rejects were recorded. For 47 of these cases, however, the operator made a retry, and all but 16 of these were accepted. All of these errors were traced to either reflections from eye wear that obscured the iris or user difficulty (e.g., difficulty in self-positioning). No false accepts were recorded. In the second phase, 96 of the people involved in the first phase attempted an identification relative to a data base with 403 entries, none of which corresponded to the operators in question. Once again, no false accepts were recorded. This study is of particular interest since of the reported iris-recognition tests, it comes closest to approximating an actual deployment of a system. In both studies of the Daugman system, operators found it to be generally unobjectionable in subjective evaluation. However, some reports of discomfort with the illuminant were recorded in the second study.

The Wildes *et al.* iris-recognition system consists of an image-acquisition rig (low light video camera, lens, framegrabber, diffuse polarized illuminator, and reticle for operator positioning) interfaced to a standard computer workstation (a Sun SPARCstation 20). The image-analysis software for the system has been implemented in the C or UNIX C Shell languages without optimization. This system is capable of two functional modes of operation: enrollment and verification. These modes operate analogously to those described for the Daugman system. Both of these modes require approximately 10 s to complete. A significant speed-up of execution should be possible,

however, via optimization of the image-analysis software. No commercial version of this system is available.

The Wildes *et al.* system has not been evaluated to the same degree as has the Daugman system. In particular, the system has been the subject of one empirical study [52]. In this study, a total of 60 different irises were represented as derived from 40 persons. For each iris, ten images were captured: five at an initial session and five approximately one month later. Of note is the fact that this sample included identical twins. Again, the common range of iris colors (blue, hazel, green, and brown) were represented. This preparation allowed for the same types of comparisons as the previously described experiments. There were no observed false positives or false negatives in the evaluation of this corpus of data. In this case, statistical analysis was eschewed owing to the small sample size. At a qualitative level, however, the data for authentic and imposters were well separated. In subjective reports, operators found the system to be unobjectionable.

Overall, the two iris-recognition systems that are being used for illustration have performed remarkably well under preliminary testing. Given that the experiments were conducted on samples on the order of 10^2 or less (i.e., number of irises in the experiments) from a population on the order of 10^{10} (i.e., total number of human irises), however, one must be cautious in the extrapolation of these results. Nevertheless, the results speak in favor of iris recognition as a promising biometric technology.

IV. CONCLUSION

For at least a century, it has been suggested that the iris can subserve biometrically based recognition of human individuals. Recent efforts in machine vision have yielded automated systems that take strides toward realizing this potential. As currently instantiated, these systems are relatively compact and efficient and have shown promising performance in preliminary testing. Extant systems require a fair amount of operator participation and work at rather close range. Therefore, they are best suited to controlled assessment scenarios (e.g., portal entry and the like).

The notion that the iris is a useful biometric for recognition stems largely from anecdotal clinical and indirect developmental evidence. This body of evidence suggests that the structure of individual irises is highly distinctive and stable with age. Empirical testing of documented iris-recognition systems provide additional support for these claims; however, these tests were limited in scope. An important direction for future efforts is the design and execution of controlled, large-scale, longitudinal studies. Only via reference to such studies can the true accuracy of iris recognition be determined for both the verification and identification tasks. Another potentially rich direction for future research would be to relax the constraints under which current iris-recognition systems operate. In this regard, it would be particularly desirable to decrease the required level of operator participation even while increasing the physical distance from which evaluation takes place. If such

goals can be achieved, then iris recognition can provide the basis for truly noninvasive biometric assessment. Further, if these enhancements can be had while maintaining compact, efficient, and low-cost implementations, then iris recognition will be well positioned for widespread deployment.

ACKNOWLEDGMENT

The author wishes to thank W. A. Richards for providing the suggestion that the author investigate the human iris as a basis for a biometric technology, P. J. Burt for discussion on the definition of Laplacian pyramids, and L. A. Raymond for generating the diagrams of iris anatomy that are shown in Fig. 2.

REFERENCES

- [1] F. H. Adler. *Physiology of the Eye*. St. Louis, MO: Mosby, 1965.
- [2] D. H. Ballard and C. M. Brown. *Computer Vision*. Englewood Cliffs, NJ: Prentice-Hall, 1982.
- [3] J. R. Bergen, P. Anandan, K. Hanna, and R. Hingorani. "Hierarchical model-based motion estimation," in *Proc. Euro. Conf. Computer Vision*, Santa Margherita Ligure, Italy, 1991, pp. 5-10.
- [4] L. Berggren. "Iridology: A critical review," *Acta Ophthalmologica*, vol. 63, pp. 1-8, 1985.
- [5] A. Bertillon. "La couleur de l'iris," *Rev. Sci.*, vol. 36, no. 3, pp. 65-73, 1885.
- [6] F. Bouchier, J. S. Ahrens, and G. Wells. "Laboratory evaluation of the IriScan prototype biometric identifier," Sandia National Laboratories, Albuquerque, NM, Tech. Rep. SAND'96-1033, 1996.
- [7] R. Bright. *Smartcards: Principles, Practice, Applications*. New York: Ellis Horwood, 1988.
- [8] P. J. Burt and E. Adelson. "The Laplacian pyramid as a compact image code," *IEEE Trans. Comput.*, vol. 31, no. 4, pp. 532-540, 1983.
- [9] R. Chellappa, C. L. Wilson, and S. Sirohey. "Human and machine recognition of faces: A survey," *Proc. IEEE*, vol. 83, pp. 705-740, May 1995.
- [10] W. T. Cope, M. L. Wolbarsht, and B. S. Yamanishi. "The corneal polarization cross," *J. Opt. Soc. Amer. A. Opt. Image Sci.*, vol. 68, no. 6, pp. 1139-1140, 1978.
- [11] J. G. Daugman. "Complete discrete 2-D Gabor transforms by neural networks for image analysis and compression," *IEEE Trans. Acoust., Speech, Signal Processing*, vol. 36, pp. 1169-1179, 1988.
- [12] ———. "Biometric signature security system," Harvard University, Cambridge, MA, Tech. Rep., 1990.
- [13] ———. "High confidence personal identification by rapid video analysis of iris texture," in *Proc. IEEE Int. Carnahan Conf. Security Technology*, 1992, pp. 1-11.
- [14] ———. "High confidence visual recognition of persons by a test of statistical independence," *IEEE Trans. Pattern Anal. Machine Intell.*, vol. 15, no. 11, pp. 1148-1161, 1993.
- [15] ———. "Biometric personal identification system based on iris analysis," U.S. Patent 5 291 560, 1994.
- [16] H. Davson. *The Physiology of the Eye*, 2nd ed. Boston, MA: Little, Brown & Co., 1963.
- [17] A. W. Drake. *Fundamentals of Applied Probability Theory*. New York: McGraw-Hill, 1986.
- [18] R. O. Duda and P. E. Hart. *Pattern Classification and Scene Analysis*. New York: Wiley, 1973.
- [19] R. A. Fisher. "The use of multiple measurements in taxonomic problems," *Annals Eugenics*, vol. 7, no. 2, pp. 179-188, 1936.
- [20] L. Flom and A. Safir. "Iris recognition system," U.S. Patent 4 641 349, 1987.
- [21] D. Gabor. "Theory of communication," *J. Inst. Elect. Eng.*, vol. 93, pp. 429-459, 1946.
- [22] S. B. Grimes and I. Kershner. *Never Say Never Again*. Warner Brothers, 1983.
- [23] K. Hanna, R. Mandelbaum, L. Wixson, D. Mishra, and V. Paragana. "A system for nonintrusive human iris acquisition,"

in *Proc. Int. Association for Pattern Recognition Workshop on Machine Vision Applications*, Tokyo, Japan, 1996, pp. 200–203.

[24] J. P. Holmes, L. J. Wright, and R. L. Maxwell, "A performance evaluation of biometric identification devices," Sandia National Laboratories, Albuquerque, NM. Tech. Rep. SAND91-0276, 1991.

[25] B. K. P. Horn, *Robot Vision*. Cambridge, MA: MIT Press, 1986.

[26] P. Horowitz and W. Hill, *The Art of Electronics*, 2nd ed. New York: Cambridge Univ. Press, 1988.

[27] P. V. C. Hough, "Method and means for recognizing complex patterns," U.S. Patent 3 069 654, 1962.

[28] J. Illingworth and J. Kittler, "A survey of the Hough transform," *Comput. Vision, Graph. Image Processing*, vol. 44, pp. 87–116, 1988.

[29] B. Jahne, *Digital Image Processing*, 2nd ed. Berlin: Springer-Verlag, 1993.

[30] N. S. Jayant and P. Noll, *Digital Coding of Waveforms*. Englewood Cliffs, NJ: Prentice-Hall, 1984.

[31] F. A. Jenkins and H. E. White, *Fundamentals of Optics*. New York: McMillan, 1976.

[32] R. G. Johnson, "Can iris patterns be used to identify people," Los Alamos National Laboratory, CA, Chemical and Laser Sciences Division, Rep. LA-12331-PR, 1991.

[33] M. Kass, A. Witkin, and D. Terzopoulos, "Snakes: Active contour models," in *Proc. Int. Conf. Computer Vision*, London, England, 1987, pp. 259–268.

[34] A. L. Kroeber, *Anthropology*. New York: Harcourt Brace Jovanovich, 1948.

[35] P. C. Kronfeld, "The gross anatomy and embryology of the eye," in *The Eye*, vol. 1. H. Davson, Ed. London: Academic, 1968, pp. 1–66.

[36] N. A. Macmillan and C. D. Creelman, *Detection Theory: A User's Guide*. Cambridge: Cambridge Univ. Press, 1991.

[37] A. Malickas, personal communication, 1994.

[38] I. Mann, *The Development of the Human Eye*. New York: Grune and Stratton, 1950.

[39] D. Marr, *Vision*. New York: Freeman, 1982.

[40] B. Miller, "Vital signs of identity," *IEEE Spectrum*, vol. 31, pp. 22–30, Feb. 1994.

[41] D. Miller, *Ophthalmology*. Boston, MA: Houghton Mifflin, 1979.

[42] F. W. Newell, *Ophthalmology Principles and Practice*, 7th ed. St. Louis, MO: Mosby, 1991.

[43] G. Olivier, *Practical Anthropology*. Springfield, IL: Charles C. Thomas, 1969.

[44] W. K. Pratt, *Digital Image Processing*. New York: Wiley, 1978.

[45] A. Samal and P. A. Iyengar, "Automatic recognition and analysis of human faces and facial expressions: A survey," *Pattern Recognit.*, vol. 25, pp. 65–77, 1992.

[46] J. E. Siedlarz, "Iris: More detailed than a fingerprint," *IEEE Spectrum*, vol. 31, p. 27, Feb. 1994.

[47] P. Sinha, "A head mounted display," Bachelor's thesis. Department of Electrical Engineering and Computer Science, Massachusetts Institute of Technology, Cambridge, 1992.

[48] J. Stotz, personal communication, 1994.

[49] W. P. Tanner and J. A. Swets, "A decision-making theory of visual detection," *Psychol. Rev.*, vol. 61, pp. 401–409, 1954.

[50] Vesalius, *De Humani Corporis Fabrica*, 1543.

[51] H. P. Wasserman, *Ethnic Pigmentation*. New York: Elsevier, 1974.

[52] R. P. Wildes, J. C. Asmuth, G. L. Green, S. C. Hsu, R. J. Kolczynski, J. R. Matey, and S. E. McBride, "A machine vision system for iris recognition," *Mach. Vision Applicat.*, vol. 9, pp. 1–8, 1996.

[53] ———, "A system for automated iris recognition," in *Proc. IEEE Workshop on Applications of Computer Vision*, Sarasota, FL, 1994, pp. 121–128.

[54] ———, "Iris recognition for security access control: Final report," National Information Display Laboratory, Princeton, NJ. Tech. Rep., 1992.

[55] R. P. Wildes, J. C. Asmuth, S. C. Hsu, R. J. Kolczynski, J. R. Matey, and S. E. McBride, "Automated, noninvasive iris recognition system and method," U.S. Patent 5 572 596, 1996.

[56] R. S. Worrall, "Iridology: Diagnosis or delusion," *The Skeptical Inquirer*, pp. 23–35, Spring 1983.

[57] A. L. Yuille, P. Hallinan, and D. Cohen, "Feature extraction from faces using deformable templates," *Int. J. Comput. Vis.*, vol. 8, no. 2, pp. 99–112, 1992.



Richard P. Wildes (Member, IEEE) received the Ph.D. degree from the Massachusetts Institute of Technology (MIT), Cambridge, in 1989.

In 1984–1988, he was a Research Assistant in the MIT Artificial Intelligence Laboratory. During that time, he was a National Science Foundation Graduate Fellow. In 1988, he joined the Department of Computer Science at the State University of New York at Buffalo as an Assistant Professor. During 1990, he joined The Sarnoff Corporation, where he is a Member of the Technical Staff. His main areas of research interest are machine and biological perception (especially vision), robotics, and artificial intelligence.